Korean J. Chem. Eng., 38(12), 2536-2540 (2021)
DOI: 10.1007/s11814-021-0946-6

pISSN: 0256-1115
eISSN: 1975-7220

Fabrication & characterization of novel conductive nanomaterial, $Ca_xCr_{0.5-x}Mg_{0.5}Fe_2O_4$

Sumaira Nosheen*,, Sadia Sagar Iqbal***, Ali Bahadar****, Nazia Hossain*****,†, and Tasawar Shahzad*****

*Department of Polymer Engineering and Technology, University of the Punjab, Pakistan
**PITMAEM, PCSIR Laboratories Complex Ferozepur Road Lahore, Pakistan
***Department of Physics, University of Lahore, Pakistan
****Department of Chemical and Materials Engineering, King Abdulaziz University, Rabigh 21911, Saudi Arabia
*****School of Engineering, RMIT University, Melbourne VIC 3001, Australia
(*Received 13 April 2021 • Revised 29 August 2021 • Accepted 31 August 2021*)

Abstract−A novel conductive nano material, nano spinel ferrites having the composition of calcium chromium magnesium nanoferrites ($Ca_xCr_{0.5-x}Mg_{0.5}Fe_2O_4$), was fabricated via sol-gel auto combustion process. The main objective was to fabricate highly stable nanocomposite as conductive material. Reaction among highly pure grade magnesium nitrate Mg $(NO_3)_2{\cdot}6H_2O$, calcium nitrate Ca $(NO_3)_2{\cdot}4H_2O$, and chromium nitrate Cr $(NO_3)_3{\cdot}9H_2O$, ferric nitrate Fe $(NO_3)_3{\cdot}9H_2O$ took place to fabricate the desired material and, later on, an inductance (L)--capacitance (C)--resistance (R) meter (LCR meter) was used to determine the conductive behavior of the material. During characterization, thermogravimetric study confirmed that the stable phase was obtained above 950 °C. Fabricated ferrite FTIR spectrum was observed between 400 cm^{-1} and 4,500 cm^{-1}. The entire sample's structural investigation was carried out employing X-ray diffraction. Morphological analysis confirmed that particles possess angular structures having acute angles adjoining surfaces. During conductivity test, all fabricated nanoferrites presented that with the increase of frequency by LCR meter, AC conductivity had been increased. The outcome of doping of calcium on chromium magnesium nanoferrites on structural in addition to dielectric properties was synergistic.

Keywords: Spinel Ferrites, X-Ray Diffraction, Thermal Analysis, FTIR, Dielectric Properties

INTRODUCTION

Nanomaterials are undergoing rapid development in recent years because of their existing and potential applications in many scientific areas, such as electronics, ceramics, biomaterials, and structural components. The particle size of the developed material is considered a key point while talking about a material's properties. This is because of reduced material size, which finally leads to rapid change in material properties [1-3]. Nanomaterials' high surface energies play a pivotal role in physical, chemical, and biomedical areas [4-6]. Nanocomposite materials composed of nanometric metal and metal oxide particles embedded in various matrices disclose various exciting electric, magnetic and catalytic properties [7-11]. The spinel ferrite structure with the formula of MFe_2O_4 (M=Co, Ni, Zn, or other metals) can be described as a cubic, closely packed arrangement of oxygen atoms, and M^{2+} and Fe^{3+} ions can occupy either tetrahedral (A) or octahedral (B) sites [12]. Spinel ferrite nanoparticles have attracted much attention because of their electronic, magnetic, and catalytic properties, which are different from their bulk counterparts.

To acquire materials with the desired physical and chemical properties, the preparation of ferrite nanoparticles through different routes has become an important area of research and development. Various methods of synthesizing spinel ferrite nanoparticles have been reported, such as ball milling, a ceramic process by firing [13], co-precipitation [14,15], reverse micelles [16], hydrothermal methods [17,18], a polymeric precursor [19], sol-gel [20], microemulsions [21], laser ablation [22], a polyol method [23], sonochemical approaches [24], and aerosol method [25]. Among these strategies, co-precipitation, as well as sol-gel, is usually renowned. Iqbal et al. [26] discussed the study of Ce^{3+} doped nano-ferrite synthesized sol-gel auto combustion method. X-ray diffraction (XRD) results revealed the spinel cubic structure and spinel cubic structure with Fourier transform infrared analysis (FTIR). Dielectric properties were augmented with the increase of doping. Nosheen et al. [27] reported the La^{3+} substituted spinel ferrites with composition $La_xMg_{0.8-x}Y_{0.2}Fe_2O_4$ were fabricated by following sol-gel auto combustion process. Structural interpretation of all synthesized nanoferrite specimens was carried out by means of XRD, scanning electron microscopy (SEM) in addition to FTIR process. Fabricated ferrite x-ray pattern confirms cubic spinel ferrite configuration. La^{3+} replacement effect on diverse fundamental criterion of yttrium magnesium ferrites was noted. Dielectric properties, for instance, dielectric constant, dielectric loss along with ac conductivity as a part of frequency on room temperature goes on mounting with incorporation of Lanthanum ion in yttrium magnesium nanoferrites. Mg-Zn nanocrystalline ferrites ($Mg_{1-x}Zn_xFe_2O_4$, were synthesized by the citrate gel auto-combustion route. XRD revealed the formation of nano-sized particles with cubic spinel structure. SEM micrographs revealed inhomogeneous grains with agglomerates. FTIR and Raman spectra recorded at room temperature confirmed the spinel structure of ferrites. The study reveals the superparamagnetic nature of the syn-

†To whom correspondence should be addressed.
E-mail: bristy808.nh@gmail.com

thesized samples, showing that the blocking temperature (TB) depends on interparticle interaction [28]. Optimum sintering temperature plays an important role in controlling densification and growth of grains, which greatly affects the magnetic and electrical properties of polycrystalline materials. Y substituted Mg-Zn[$Mg_{0.5}Zn_{0.5}Y_xFe_{2-x}O_4$ ($0 \le x \le 0.05$)] ferrites have been prepared by using conventional standard ceramic technique. Characterization of the samples analyzed and the results confirmed the same information regarding phase analysis at different Impedance spectroscopy also exhibiting similar trend as ac-electrical resistivity. The initial permeability revealed the wide stability zone of frequency. The ac resistivity values were higher for bulk density and permeability. The effect of sintering temperature on the physical properties of Y-substituted $Mg_{0.5}Zn_{0.5}Y_xFe_{2-x}O_4$ ferrites was improved [29].

In the present research, the calcium doping effect on structural properties of Cr-Mg nano spinel ferrites formulated by the sol-gel method has been investigated. The main objective of this study was to fabricate highly stable nanocomposite as the conductive material. Therefore, the designed conductive nanostructure spinel ferrites material was characterized by thermogravimetric analysis (TGA), FTIR, SEM, XRD, and impedance studies. The multifunctional prepared nano-ferrites would be applicable in different fields, including optoelectronics, magnetic recording media, security switching applications.

MATERIALS AND METHODS

1. Materials

Nanoferrites with stoichiometric composition $Ca_xCr_{0.5-x}Mg_{0.5}Fe_2O_4$ where x varies from 0-0.5 with the interval of 0.1 were fabricated via sol-gel auto combustion approach. For this purpose, nitrate salt purchased from Sigma Aldrich (as high purity) including magnesium nitrate Mg $(NO_3)_2 \cdot 6H_2O$, calcium nitrate Ca $(NO_3)_2 \cdot 4H_2O$, chromium nitrate Cr $(NO_3)_3 \cdot 9H_2O$, ferric nitrate Fe $(NO_3)_3 \cdot 9H_2O$, ammonium hydroxide, and ethylene glycol.

2. Sample Preparation

Salts of calcium, magnesium, chromium and iron nitrate were weighed to the stoichiometric amount and dissolved in 100 ml ethanol on continuous stirring and heating at 50 °C. We added 20 ml 3 M NH_4OH solution after 30 minutes and enhanced temperature to 100 °C and after that, added 1 ml PEG. Later, the temperature was increased to 220 °C, further adding 10 ml NH_4OH. After half an hour, we stopped stirring, moreover increased the temperature to 235 °C. For completion, the entire reaction took approximately 3 hours. Subsequently, samples were ground into fine powders then placed in a furnace for sintering.

3. Characterization Techniques

Synthesized $Ca_xCr_{0.5-x}Mg_{0.5}Fe_2O_4$ ferrite samples were annealed at 800 °C for 8 hours. Structural study of sintered nano-ferrites was performed by powder X-ray diffraction technique at room temperature by Cu Kα (λ=1.5406 Å) radiation with 2-theta in the range of 20-60° by using D/MAX2400 diffractometer. The wide-angle powder test employed a scanning speed of 6°/min, step width 0.04° with voltage 50 kV, current 150 mA. Ferrite powder morphology is studied by scanning electron microscopy (SEM, JSM 6940A, Jeol, Japan). Perkin Elmer Diamond 100 TG/DTA, Japan, was used to analyze the thermal degradation and endothermic/exothermic response of the nanostructure-designed ferrites within the temperature span 25-1,000 °C at a heat integrated −10 °C/min in ambient atmosphere. Absorption band spectroscopic analysis was completed by FTIR (Perkin Elmer). 10mm diameter pellets of designed nanostructure ferrites were used for calculating the complex permittivity (ε' and ε'') and dielectric tangent loss (tan δ) by RF impedance/material analyzer (Agilent E4991A) in the frequency range of 1 MHz-1 GHz. The AC conductivity can also be calculated using the values of frequency and dielectric loss factor.

RESULTS AND DISCUSSION

1. TGA

TGA assesses mass loss (%) of a sample due to the increase in temperature. This method was used for determining the phase configuration and degeneration response display in the specimen. TGA curve for $Ca_xCr_{0.5-x}Mg_{0.5}Fe_2O_4$ ferrite is represented in Fig. 1. TGA was carried out in oxygen atmosphere from room temperature to 950 °C. The initial phase of weight loss was in the range of room temperature to 150 °C, resulting from moisture loss in nanopow-

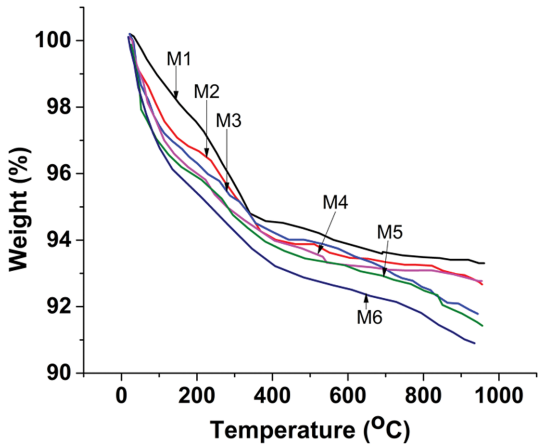

Fig. 1. Thermal reliability response against temperature from 25-950 °C of designed nanoferrites.

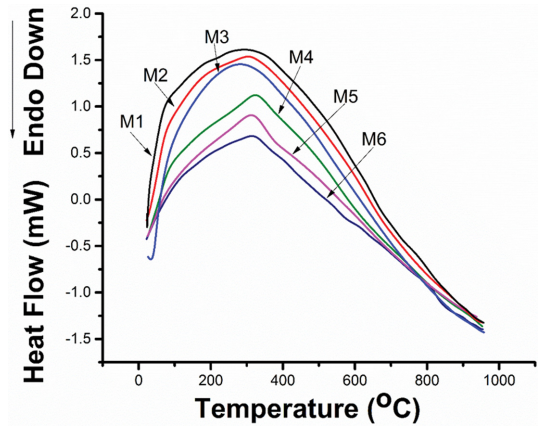

Fig. 2. Heat flow response against temperature ranging room temperature to 950 °C of designed nanoferrites.

der. The next step ended at 400 °C, which is linked with nitrate ignition and remaining carbon-based entities. Later, no additional foremost weight loss was noticed ascertaining the existence of merely chromium magnesium ferrites as well as calcium doped chromium magnesium ferrites up to 950 °C.

Nanoferrite sample differential thermal analysis was performed at temperature ranging from 25 °C-950 °C in an oxygen environment The assembled information is represented in Fig. 2. DTA curves explain exothermic conduct from 100-300 °C owing to evaporation as well as hot gas exhaust. Subsequently, an endothermic process advanced followed employing heat absorption; however, there was no extra altering of the nature of phases. This confirms that nanoferrites are incredibly dense with much fewer air voids (pores). Configuration of remarkably perfect $Ca_xCr_{0.5-x}Mg_{0.5}Fe_2O_4$ ferrite was obtained from TGA/DTA outcome. Assist, it is confirmed via FTIR, XRD as well as SEM study.

2. Morphological Study

To examine nanopowder morphology, particle configuration/magnitude, a scanning electron microscope was utilized. Fig. 3(a) presents micrographs of fabricated chromium magnesium ferrites and calcium doped chromium magnesium ferrite nanopowder ($Ca_xCr_{0.5-x}Mg_{0.5}Fe_2O_4$) through changing x from 0-0.5 with a gap of 0.1 with polyethylene glycol as the chelating agent. In SEM micrographs, fabricated nanoferrites have an angular configuration possessing acute angle neighboring surfaces. Alternatively, doping calcium particles depict further irregular shapes and massive clusters because of agglomeration in Fig. 3((b), (c), (d), (e), (f)).

3. XRD Study

XRD analysis was used to verify the nanostructure of synthesized nanoferrite specimen ($Ca_xCr_{0.5-x}Mg_{0.5}Fe_2O_4$), as revealed in Fig. 4. The cubic spinel phase structure is affirmed by International Center for Diffraction Data by card #01-073-1720. Strong evidence for assembly of spinel arrangement of ferrites is matched up with diffraction peaks of associated planes (220), (222), (311), (400), (440), (422), and (511). The nanosize of fabricated nanoferrites is an obvious sign from the broad peak in XRD patterns. To calculate nanoferrite average crystallite size (D), Debye Scherer's formula is utilized via noticing widened peaks with high intensity (311). Calcium ions generally exist at B octahedral position. Cation allocation is verified from the lattice constant of theoretical assessment. This displays good union with experimental as well as ICDD cards of related nanoferrites.

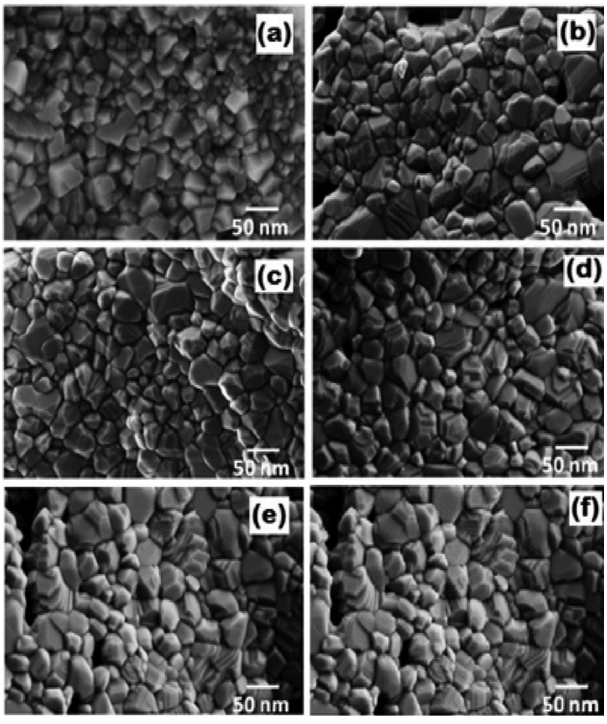

Fig. 3. SEM micrographs of $Ca_xCr_{0.5-x}Mg_{0.5}Fe_2O_4$ ferrite nanostructure with varying x value from x=0.0, x=0.1, x=0.2, x=0.3, x=0.4, and x=0.

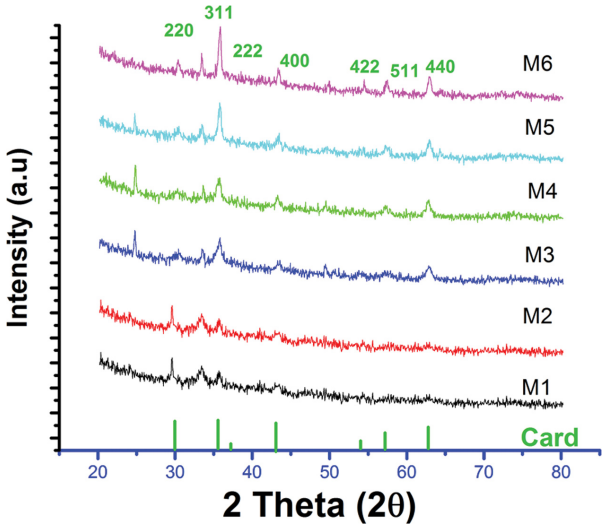

Fig. 4. XRD pattern of $Ca_xCr_{0.5-x}Mg_{0.5}Fe_2O_4$ ferrite nanostructure with varying x value from x=0.0, x=0.1, x=0.2, x=0.3, x=0.4, and x=0.5.

4. FTIR Analysis

FTIR band of fabricated nanoferrites with doping of calcium is represented in Fig. 5. B octahedral metal vibration stretching occurs at 500-700 cm^{-1}, and at 800-900 cm^{-1}, absorption max out is correlated to metal vibration stretching at the tetrahedral position. Oxide lattice vibrations against cations emerge at 1,000-1,200 cm^{-1}. From the FTIR spectrum, it is apparent that absorption bands of dried gel at 3,200 cm^{-1} are significant signatures of the O-H bond. Adsorption of CO_2 from the environment is acquired at 2,395 cm^{-1}. The existence of the carboxyl group and traces of NO_3^- ions at 1,629 and 1,394 cm^{-1} in the position of absorption bands correspond to stretching vibration, respectively. However, bands at 1,068, 825, and 640 cm^{-1} are connected with the deformation of the C-H group because of the stretching vibration band.

5. Dielectric Constant

Dielectric constants of all ferrites were computed from the frequency range 20 Hz-5 MHz, as shown in Fig. 6. The figure depicts the variation of dielectric constant with frequency for different concentrations of calcium ions. It is apparent that nanoferrites display dielectric allocation where the drop in dielectric constant (ε) takes place with a rise of frequency from 20 Hz-5 MHz. The rapid decline in dielectric constant occurs in the less frequency segment

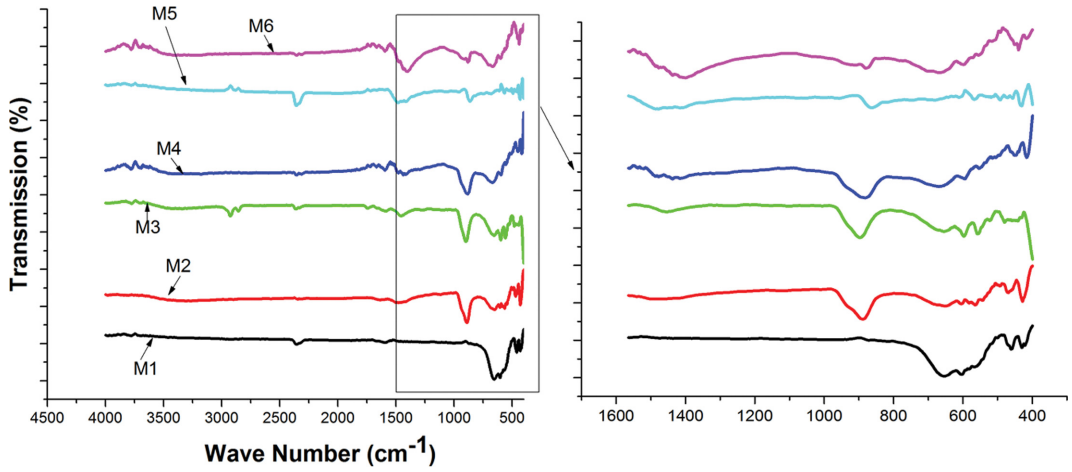

Fig. 5. FTIR Spectra of designed nanoferrites.

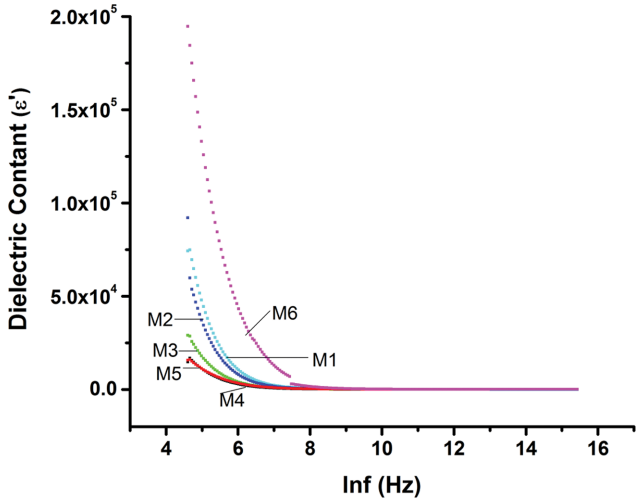

Fig. 6. Dielectric constant vs. lnf of designed nanoferrites.

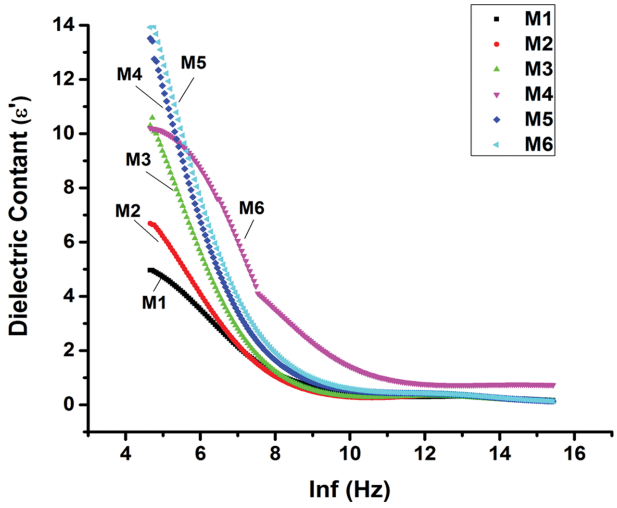

Fig. 7. Dielectric loss factor vs. lnf of designed nanoferrites.

and decreases in the high-frequency segment, and practical methodologies are independent of frequency. In ferrite samples, dielectric dispersal has been elaborated on the root of Maxwell-Wagner model and Koop's phenomenological theory of dielectrics [12-14]. Maxwell-Wagner model suggests that the dielectric medium comprises superior conducting particles, which are distinct by less conducting particle borders. It was observed that in ferrites, permittivity has a direct link to the square root of conductivity [15].

Consequently, particles have enhanced conductive and permittivity values, while particle borders are less conductive and present lower permittivity values. At lesser frequencies particle borders are more valuable than particles in electrical transmission. Thinner particle border--advanced is the value of dielectric constant. Upper dielectric constant (ε') matters noticed at lower frequencies are also elaborated on interfacial/space polarization because of inhomogeneous dielectric configuration [16,18].

6. Dielectric Loss

Homogeneities in the system can be detected based on porosity and particle arrangement. The dielectric loss tangent is presented in Fig. 7. It is apparent that through the increase in frequency, the loss tangent decreases, followed by the emergence of a relaxation peak. Debye relaxation theory is practical to clarify the existence of relaxation peak. The current study presents a relaxation peak at frequency 450 kHz and shifted towards lower frequency with increased calcium ion amount. Relaxation peak shifting from higher to lower frequency area with an increase in Ca^{2+} discloses the enhancement of dipole-dipole interactions, which ground obstacle to the rotation of dipoles. For this reason, resonance among the rotation of dipoles and applied field happens at a lower frequency. Fallout represents a decrease in dielectric constant as well as loss tangent with the increase in Ca^{2+} quantity.

7. AC Conductivity

For conductivity study of ferrites, sample porosity, compactness, grain margin, chemical makeup, and particle size are significant factors that are accountable. Frequency reliant AC conductivity means plus calcium doped chromium magnesium nanoferrites are portrayed in Fig. 8. For all fabricated nanoferrites, increase in AC conductivity is noticed with the increase in frequency. This is

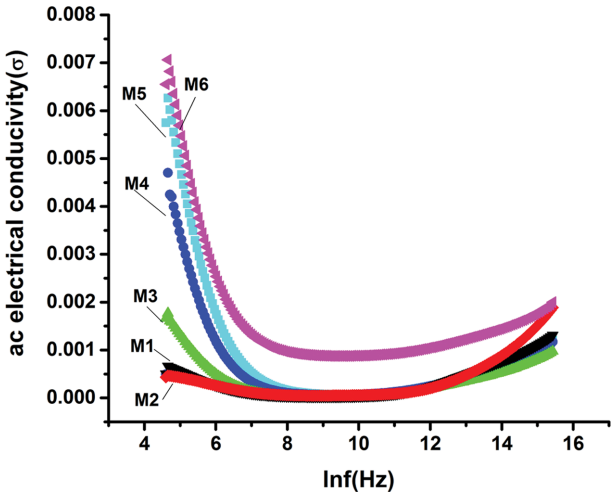

Fig. 8. AC conductivity against lnf of designed nanoferrites.

a result of the movement of the charge carrier since the field is applied. From Fig. 8, it is observed that with the increase of frequency, the hopping of charge carrier is improved and cause of boost in conductivity. However, at low frequency, AC conductivity is not elevated because of resistive grain margins that are the basis for the opposition of electron movement.

Conversely, at higher frequencies, conductivity increases due to the movement of electrons that holds swiftly due to active conductive particles due to the movement of electrons that hold new charge carriers from diverse sites. It is clear from the response that AC conductivity is enhanced with calcium concentration at room temperature. An increase in AC conductivity took place since calcium has less resistivity than chromium. Alteration in the conduction mechanism is because of the movement of hopping holes that cause reduction and increase in conductivity.

CONCLUSION

The sol-gel auto combustion approach was used for the successful synthesis of designed $Ca_xCr_{0.5-x}Mg_{0.5}Fe_2O_4$ nanoferrites. The variation in structural, electrical and dielectric properties was observed for $Ca_xCr_{0.5-x}Mg_{0.5}Fe_2O_4$ ferrites nanostructures with varying x value from x=0.0, x=0.1, x=0.2, x=0.3, x=0.4, and x=0.5. XRD analysis confirmed the formation of a single-phase cubic spinel structure with the space group Fd3m for all synthesized samples. SEM images reveal particles in the nanosized range. Moreover, thermograms and differential thermal contours showed the stability of $Ca_xCr_{0.5-x}Mg_{0.5}Fe_2O_4$ nanoferrites. The complex impedance spectra of all ferrites nanostructures show only one semicircular arc, suggesting a principal role of the grain boundary contribution. The decrease in dielectric constant with increasing frequency was observed, which may be attributed to the Maxwell-Wagner polarization and conduction mechanism in these nanostructured ferrites. The AC conductivity increased with frequency. The experimental results reveal that synthesized materials are highly porous and exhibit their size at the nanoscale. They are useful in applications to reducing noise ratio, gas sensors, and nanoelectronic devices.

REFERENCES

1. M. Ali, M. Khan, F. U. Z. Chowdhury, M. Hossain, M. Rahman, S. Hoque, M. Martin and M. Uddin, *Results Phys.*, **14**, 102517 (2019).
2. B. Alibeiki, P. Kameli, H. Salamati, M. Eshraghi and T. Tahmasebi, *J. Magn. Magn.*, **322**, 2929 (2010).
3. S. A. Bagherzadeh, A. D'Orazio, A. Karimipour, M. Goodarzi and Q.-V. Bach, *Phys. A: Stat. Mech. Appl.*, **521**, 406 (2019).
4. G. Baldi, D. Bonacchi, C. Innocenti, G. Lorenzi and C. Sangregorio, *J. Magn. Magn.*, **311**, 10 (2007)
5. V. L. Calero-DdelC and C. Rinaldi, *J. Magn. Magn.*, **314**, 60 (2007).
6. L. Chen, Y. Shen and J. Bai, *Mater. Lett.*, **63**, 1099 (2009).
7. A. Corrias, M. F. Casula, A. Falqui and G. Paschina, *J. Mater. Chem.*, **16**, 3130 (2004).
8. M. Gharagozlou, *J. Alloys Compd.*, **486**, 660 (2009).
9. A. Ghasemi, M. Hassani, M. Goodarzi, M. Afrand and S. Manafi, *Phys. A: Stat. Mech. Appl.*, **514**, 36 (2019).
10. S. S. Iqbal, A. Bahadar, N. Hossain, N. Gull, T. S. Ahmad, N. Ehsan, S. U. Khan and T. Riaz, *J. Environ. Chem. Eng.*, **9**, 106085 (2021).
11. M. Khedr, A. Omar and S. Abdel-Moaty, *Colloids Surf. A Physicochem. Eng. Asp.*, **281**, 8 (2006).
12. S. Khorrami, F. Gharib, G. Mahmoudzadeh, S. S. Sepehr, S. S. Madani, N. Naderfar and S. Manie, *Int. J. Nano Dimens*, **1**, 221 (2011).
13. D. R. Kumar, S. I. Ahmad, C. A. Lincoln and D. Ravinder, *J. Asian Ceram. Soc.*, **7**, 53 (2019).
14. W. Liu, O. Malekahmadi, S. A. Bagherzadeh, M. Ghashang, A. Karimipour, S. Hasani, I. Tlili and M. Goodarzi, *Int. Commun. Heat Mass Transf.*, **109**, 104333 (2019).
15. S. A. Mazari, E. Ali, R. Abro, F. S. A. Khan, I. Ahmed, M. Ahmed, S. Nizamuddin, T. H. Siddiqui, N. Hossain, N. M. Mubarak and A. Shah, *J. Environ. Chem. Eng.*, **9**, 105028 (2021).
16. S. A. Mazari, N. Hossain, W. J. Basirun, N. M. Mubarak, R. Abro, N. Sabzoi and A. Shah, *Process Saf. Environ. Prot.*, **149**, 67 (2021).
17. S. Nosheen, S. S. Iqbal, P. Shahzadi, A. Sabir, R. Khan and T. Shahzad, *European J. Adv. Eng. Technol.*, **7**, 32 (2020).
18. E. Pervaiz and I. Gul, *J. Phys. Conf. Ser., IOP Publishing*, 012015 (2013).
19. V. Pillai and D. Shah, *J. Magn. Magn.*, **163**, 243 (1996).
20. A. D. Pogrebnyak, A. P. Shpak, N. A. Azarenkov and V. M. Beresnev, *Phys-USP*, **52**, 29 (2009).
21. K. V. Shafi, A. Gedanken, R. Prozorov and J. Balogh, *J. Mater. Chem.*, **10**, 3445 (1998).
22. A. Shahsavar, S. Khanmohammadi, A. Karimipour and M. Goodarzi, *Int. J. Heat Mass Transf.*, **131**, 432 (2019).
23. J. B. Silva, W. De Brito and N. D. Mohallem, *Mater. Sci. Eng. B*, **112**, 182 (2004).
24. P. Silva, V. Sagredo, W. Bramer, E. Perez and F. Torres, *J. Phys. Conf. Ser., IOP Publishing*, 082023 (2010).
25. G. Xiao and C. Chien, *Appl. Phys. Lett.*, **51**, 1280 (1987).
26. R. Zakir, S. S. Iqbal, A. U. Rehman, S. Nosheen, T. S. Ahmad, N. Ehsan and F. Inam, *Ceram. Int.*, **47**, 20 (2021).
27. J. Zhang and C. Q. Lan, *Mater. Lett.*, **62**, 1521 (2008).
28. D. Zhao, X. Wu, H. Guan and E. Han, *J. Supercrit. Fluids*, **42**, 226 (2007).
29. Z. Zi, Y. Sun, X. Zhu, Z. Yang, J. Dai and W. Song, *J. Magn. Magn.*, **321**, 1251 (2009).